Published March 4, 2016

Original Research

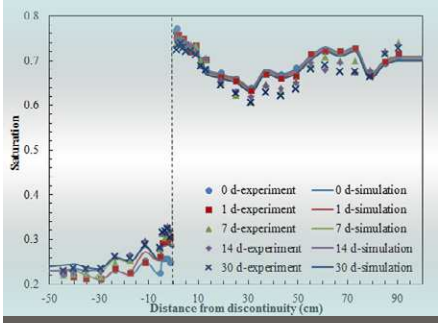

Modeling of Horizontal Water Redistribution in an Unsaturated Soil

Luwen Zhuang, S. Majid Hassanizadeh,* Martinus Th. van Genuchten, Anton Leijnse, Amir Raoof, and Chaozhong Qin

When two soil samples with the same hydraulic properties but different initial water saturations are brought into contact, water will redistribute horizontally between the samples until some equilibrium is reached. The part with a higher initial saturation undergoes drainage while imbibition occurs in the other part. Hysteresis will not allow water to redistribute evenly between the two parts. In this study we used two different modeling approaches to analyze a recent experiment related to the water redistribution process. In one approach, we assumed applicability of the standard Richards equation with a hysteretic capillary pressure–saturation relationship (including scanning curves). This approach assumes continuity in the water pressure and flux across the contact surface between the two sides. In the second approach, we used an extended two-phase flow formulation based on rational thermodynamics principles and involving the air–water specific interfacial area. For this approach, we used continuity in the Gibbs free energy for air–water interfaces and the interfacial area flux as additional conditions at the contact surface. We employed two different initial conditions: uniform initial saturation for each side and slightly nonuniform initial saturation distributions consistent with the measured water contents. We compared results of both models with measurements. The Richards equation with full hysteresis could not reproduce the measured saturation distribution unless an unrealistic value of the imbibition retention curve was assigned. The interfacial area model compared well with the experimental data after optimization of some of the model parameters.

Core Ideas

- A recent laboratory experiment of horizontal water redistribution was simulated.
- Two different models were separately used to reproduce the measured data.
- Interfacial area model results showed better agreement with experimental data.

L. Zhuang, S.M. Hassanizadeh, M.Th. van Genuchten, A. Raoof, and C. Qin, Dep. of Earth Sciences, Utrecht University, Budapestlaan 4, 3584 CD Utrecht, The Netherlands; S.M. Hassanizadeh, Soil and Groundwater Systems, Deltares, The Netherlands; M.Th. van Genuchten, Dep. of Mechanical Engineering, Federal University of Rio de Janeiro, Rio de Janeiro, Brazil; A. Leijnse, Dep. of Soil Physics and Land Management, Wageningen University, Wageningen, The Netherlands. *Corresponding author (S.M.Hassanizadeh@uu.nl).

Vadose Zone J.
doi:10.2136/vzj2015.08.0109
Received 5 Aug. 2015.
Accepted 19 Nov. 2015.

The process of moisture redistribution in soils has attracted much attention because of its importance to many practical problems in soil science, hydrology, and agricultural engineering as well as for various porous media processes in industry. Similar redistribution processes in multifluid systems occur in petroleum engineering and carbon sequestration problems. Starting with early studies by Always and Clark (1911), Haines (1930), and especially Youngs (1958), many have focused on the vertical redistribution of water following infiltration (e.g. Biswas et al., 1966; Staple, 1969; Peck, 1971; Vachaud and Thony, 1971; Talsma, 1974; Youngs and Poulovassilis, 1976). A limited number of studies also investigated horizontal redistribution processes in homogeneous soils (Vachaud, 1969; Kona, 1997; Feuring et al., 2014) or analytically (Philip, 1964). These studies revealed different moisture distributions within the dry and wet parts of the porous media presumably caused by macroscopic hysteresis in the soil hydraulic properties.

Many empirical and approximate theoretical models have been used to describe hysteresis in the soil hydraulic properties. Empirical descriptions include those by Dane and Wierenga (1975), Scott et al. (1983), Kool and Parker (1987), Parker and Lenhard (1987), and Luckner et al. (1989). Theoretical approaches include various independent and dependent domain models such as those described by Everett (1954), Poulovassilis (1962), Philip (1964), Topp (1971), Mualem (1974, 1984), and Poulovassilis and El-Ghamry (1978). Useful reviews of different approaches and comparisons with experimental data are given by Jaynes (1984) and Pham et al. (2005).

The various approaches above are based on relatively standard formulations involving the Richards equation for variably saturated flow or related models for multiphase systems. Application of these formulations to transient redistribution processes requires the use of hysteretic relationships for the constitutive (soil hydraulic) functions. An alternative approach is based on thermodynamic principles that consider the effects of specific interfacial area on fluid flow (Hassanizadeh and Gray, 1990). While many numerical studies have been performed to investigate the general properties of this theory (Niessner and Hassanizadeh, 2008; Pop et al., 2009; Marshall, 2009; Joekar-Niasar and Hassanizadeh, 2011), the approach has never been used to analyze experimental data.

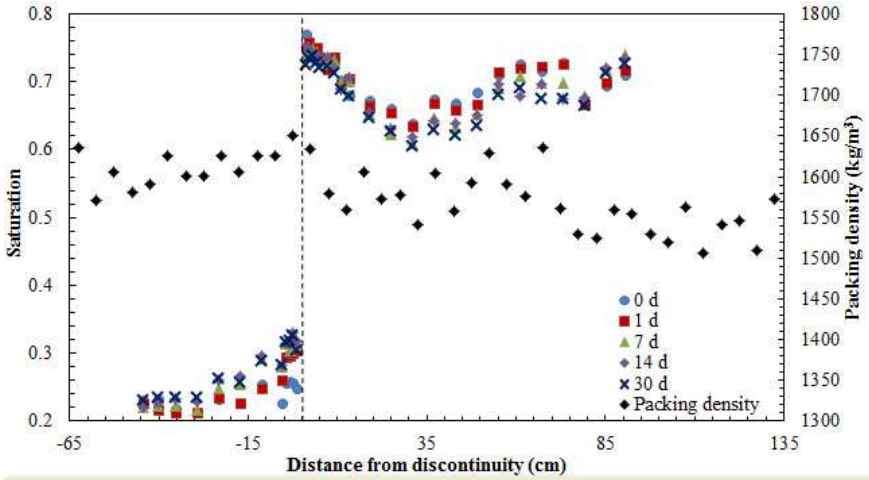

Fig. 1. Measured packing density (black diamonds) and saturation profiles at different times (other symbols) along the flume (Feuring et al., 2014).

In this work, we used results of recent horizontal redistribution experiments performed by Feuring et al. (2014) to investigate the applicability of the thermodynamics-based model of Hassanizadeh and Gray (1990), which we refer to as the interfacial area model. We simulated the experiments of Feuring et al. (2014) using two different approaches: the standard Richards equation with and without capillary hysteresis effects and the extended Darcy model that includes the air–water interfacial area. Below, we first provide a brief overview of the horizontal redistribution experiment of Feuring et al. (2014). Subsequently, we describe the standard and interfacial area models used in our study and compare the modeling results with the experimental data.

Description of Experiments of Feuring et al.

The experiments by Feuring et al. (2014) were designed to observe water redistribution in a long horizontal homogeneous soil flume with a discontinuity in initial saturation. They used a flume with dimensions of 200 (length) by 3 (height) by 4 cm (width). The flume was packed with sand having a mean grain diameter of 0.29 mm and with minimum and maximum grain sizes of 0.05 and 2 mm, respectively. Initial water saturation along the flume was not uniform: one part, covering 65 cm ($-65 \leq x < 0$), had a relatively low saturation (average of 0.23), while the remaining 135 cm ($0 < x \leq 135$) was relatively wet (average of 0.70). The particle density was 2546 kg m^{-3}, and the average packing bulk density was 1.65 kg m^{-3}. Bulk densities along the flume were measured destructively every 5 cm after the flow experiment was terminated. Results in Fig. 1 indicate that bulk densities fluctuated slightly along the flume and hence, that the flume was not perfectly homogeneous. These results were also used to calculate porosity.

The capillary pressure saturation curves for primary drainage and main imbibition were measured by Feuring (2010). Figure 2 shows the measured data along with the fitted curves used in our calculations. As can be seen, residual air saturation was found to be negligible. The primary drainage curve, hence, coincided with the main drainage curve. We will further refer to this curve as the main drainage curve. The saturated hydraulic conductivity (K_s) was also measured, using a constant head permeameter, and was found to be 6.38×10^{-4} m s^{-1}, or 55.12 m d^{-1} (Feuring et al., 2014). The measurement of K_s was repeated recently, and the same value was found. Various soil physical and hydraulic parameter values are summarized in Table 1.

The dry and wet sides of the flume were initially separated by a very thin (0.044 mm) removable metal sheet. The entire system was made airtight. Both sides were first allowed to reach equilibrium, after which the sheet was removed to start the redistribution process. Saturation

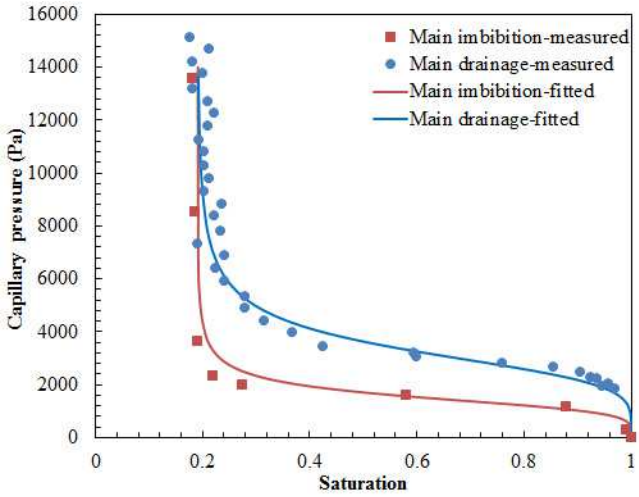

Fig. 2. Measured and fitted van Genuchten main drainage and imbibition curves (Feuring, 2010).

Table 1. Measured soil properties and parameter values.

Parameter	Unit	Value
Particle density, ρ_s	kg m^{-3}	2546
Packing bulk density, ρ_b	kg m^{-3}	1650
Average porosity, φ	–	0.4
Water density, ρ_w	kg m^{-3}	998.2
Water viscosity, μ_w	Pa·s	1×10^{-3}
Main drainage retention exponent, n	–	5.0
Main drainage retention parameter, α	m^{-1}	3.26
Main imbibition retention exponent, n	–	5.0
Main imbibition retention parameter, α	m^{-1}	6.94
Residual water saturation, S_{wr}	–	0.19
Saturated hydraulic conductivity, K_s	m s^{-1}	6.38×10^{-4}
Intrinsic permeability, K	m^2	6.52×10^{-11}

values and air and water pressures along the flume were measured before the sheet was removed and then repeatedly during a period of 30 d afterward. Water and air pressures were measured with hydrophilic and hydrophobic tensiometers, respectively. Transducer pairs were installed at 12 locations along the flume. The air pressure presented very little variation along the flume and, hence, was assumed to be constant. In our numerical studies, we assumed the air pressure to be atmospheric. Saturation along the flume was monitored using a γ-radiation system. For the calculation of saturation, the γ measurements had to be recalibrated based on measured values of the bulk density of the soil. These were measured destructively after the experiment terminated. The soil in the flume was subsequently collected in 5-cm segments to obtain precise gravimetric measurements of the bulk density along the flume. Measured saturation profiles at six different times are shown in Fig. 1 (Feuring et al., 2014). Figures 3a and 3b display measured water pressures as a function of time at various points in the initially dry and wet sides, respectively. The tensiometer at −1 cm malfunctioned during the entire experiment, while the tensiometer at −6 cm stopped working properly after 15 d. Erroneous data from these two tensiometers are not included in Fig. 3.

Figure 1 shows that saturation values increased rapidly in the dry side ($x < 0$) within 7 d, after which, moisture redistribution slowed down substantially. By comparison, saturation in the wet side ($x > 0$) decreased gradually and almost evenly along the entire subdomain. This was due to the much higher unsaturated hydraulic conductivities in the wet side, which led to very small pressure head gradients. As seen in Fig. 1, the saturation discontinuity at the contact surface between the two domains (at $x = 0$) persisted during the entire experiment. In the dry side, water pressures at positions near the contact surface increased rapidly, while pressures started to increase much later and much slower farther away from the contact surface (see Fig. 3). By comparison, water pressures in the wet side decreased only slightly and more uniformly. Although changes in the water pressure with time had not completely ceased after 1 month, the experiment was terminated, since

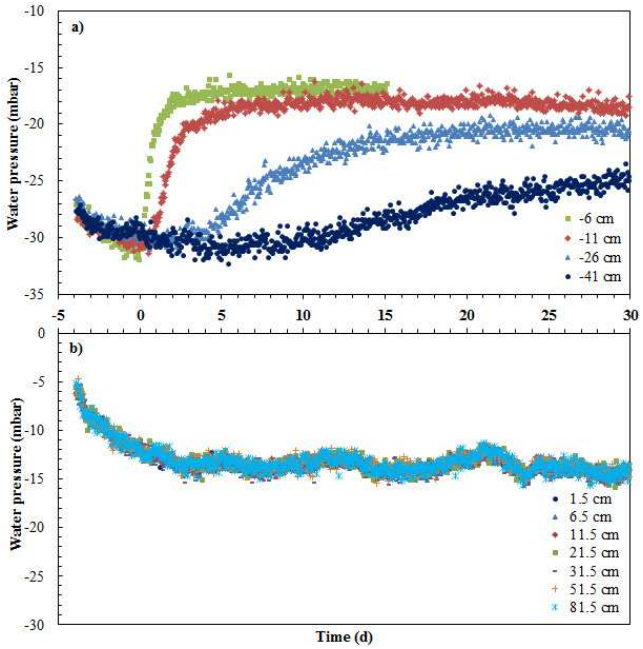

Fig. 3. Water pressure vs. time at several locations within the initially (a) dry and (b) wet sides of the flume (Feuring et al., 2014).

changes in saturation were no longer measurable. The total water mass balance was evaluated gravimetrically before and after the experiments. A loss of only 7% water was found.

Numerical Models

In the following, we describe two alternative modeling approaches for analysis of the experimental data of Feuring et al. (2014). Both modeling approaches neglect any influence of the air phase, since few variations were observed in the air pressure along the flume.

Standard Model

The HYDRUS-1D software package of Šimůnek et al. (2013) was used to simulate the horizontal redistribution experiment of Feuring et al. (2014). HYDRUS-1D uses the finite element method to solve the Richards equation for water flow in an unsaturated porous medium. For one-dimensional horizontal flow, the Richards equation reduces to the following:

$$\phi\frac{\partial S_w}{\partial t} = \frac{\partial}{\partial x}\left[K(S_w)\frac{\partial h}{\partial x}\right] \quad [1]$$

where S_w is saturation, φ is porosity, h is the soil water pressure head defined as $h = p_w/\rho_w g$, with p_w and ρ_w being the water pressure and density, respectively, K is the unsaturated hydraulic conductivity (assumed to be a function of the pressure head), t is time, and x is the spatial coordinate.

Formulas suggested by van Genuchten (1980) equations were used to characterize the nonlinear relationships between h and S_w and between K and S_w as follows:

$$h = -\frac{1}{\alpha}\left[S_e^{-1/m} - 1\right]^{1/n} \quad [2]$$

$$K(S_w) = K_s S_e^l \left[1 - \left(1 - S_e^{1/m}\right)^m\right]^2 \quad [3]$$

$$S_e = \frac{S_w - S_{wr}}{1 - S_{wr}} \quad [4]$$

where S_{wr} and S_e are the residual and effective water saturations, respectively, α and n are fitting parameters, $m = 1 - 1/n$, and $l = 0.5$. Figure 2 compares the measured and fitted capillary pressure saturation curves for main drainage and imbibition. A good fit was found, with the hydraulic parameter α for imbibition being approximately twice the value for drainage (see Table 1) as is often assumed in unsaturated flow studies (e.g., Luckner et al., 1989).

Hysteresis in HYDRUS-1D is simulated by means of scanning curves that are obtained by scaling the main imbibition and drainage curves. Every individual nodal point in the numerical model is assigned its own set of scanning curves, which are used depending on whether drying or wetting occurs. In our study, we used the approach of Lenhard and Parker (1991) to generate the various scanning curves. Their method assumes closure of the scanning loops by forcing the scanning curves to pass through the latest imbibition or drainage reversal points thus avoiding so-called artificial pumping errors (Werner and Lockington, 2006; Šimůnek et al., 2009). Consistent with the simplified hysteresis formulations by Kool and Parker (1987), Luckner et al. (1989), and Lenhard and Parker (1991), we used for all scanning curves the same values of α and n (the former depending on imbibition or drainage) but different values for porosity and residual water saturation. We later used the measured bulk densities, as shown in Fig. 1, in some of the simulations to slightly adjust the values of porosity along the entire domain. This was done to account more precisely for the packing heterogeneity.

For the simulations with HYDRUS-1D, we assigned 400 elements distributed evenly over the entire flow domain (2 m). A small grid spacing was selected to render numerical dispersion of the wetting front negligible. No-flow boundary conditions were applied to both ends of the flume, while pressure heads and water fluxes were assumed to be continuous across the contact surface. The initial condition could be defined in terms of either saturation or pressure head. We performed two sets of simulations assuming either a homogeneous or heterogeneous porous medium as follows:

1. Uniform saturation values were assigned to each side (dry or wet) with a discontinuity at the contact surface. The capillary pressure saturation curves (the main curves as well as the scanning curves) were assumed to be the same for all elements. The saturation values were based on the means of the measured initial saturations of the wet and dry sides.
2. Nonuniform measured water saturation or pressure head values were assigned as initial conditions along each side. Different porosity values and capillary pressure saturation curves (the main or scanning curves) were assigned to different sections along the flume consistent with the measured bulk densities shown in Fig. 1.

Interfacial Area Model

The capillary pressure (p_c)–saturation (S_w) relationship (or water retention curve) used in the standard Richards equation depends on the flow history and, hence, is not a unique function. Rather than resorting to a hysteretic relationship, Hassanizadeh and Gray (1993b) suggested that nonuniqueness in the capillary pressure–saturation relationship can be modeled by introducing the air–water specific interfacial area into the formulation. The air–water specific interfacial area, denoted by a_{wa}, is defined as the total area of all air–water interfaces within a unit volume of the porous medium. The approach would then involve a three-dimensional surface relating interfacial area with capillary pressure and saturation (Hassanizadeh and Gray, 1993a). Projection of this surface onto the p_c–S_w plane would form the hysteresis loop of the primary (or main) drainage and imbibition curves. Several experimental and modeling studies have suggested that the saturation–capillary pressure interfacial area surface is indeed unique for all drainage and imbibition equilibrium points, whether on the main or on scanning curves (e.g., Held and Celia, 2001; Chen and Kibbey, 2006; Chen et al., 2007; Joekar-Niasar et al., 2008; Joekar-Niasar and Hassanizadeh, 2011, 2012; Karadimitriou et al., 2014).

The three-dimensional p_c–S_w–a_{wa} surface for a given soil must be obtained experimentally. In the experiments of Feuring et al. (2014), only the main drainage and imbibition curves were measured. For this reason, we tried to develop a p_c–S_w–a_{wa} relationship in such a way that its projection onto the p_c–S_w plane would reproduce the measured p_c–S_w curves. To do so, we had to estimate values of the specific interfacial area corresponding to measured p_c–S_w data points of the drainage and imbibition curves. We followed the method of Niemet et al. (2002) to calculate specific interfacial areas. The resulting p_c–S_w–a_{wa} points were fitted with the following power function proposed by Joekar-Niasar and Hassanizadeh, 2012):

$$a_{wa}(S_w, p_c) = a S_w (1 - S_w)^b p_c^c \quad [5]$$

$$p_c = p_a - p_w \quad [6]$$

where p_c and p_a are the capillary and air pressures, respectively, and a, b, and c are empirical parameters. Equation [5] restricts the interfacial area to the physical range where water saturation varies between zero and one. The fitted surface area and its parameters are given in Fig. 4 and Table 2, respectively. The black dots in Fig. 4 correspond to p_c–S_w–a_{wa} points obtained using the approach of Niemet et al. (2002). We note that dynamic capillarity effects are neglected in Eq. [6].

Next, we introduce the generalized Darcy's law. Hassanizadeh and Gray (1993b) found that the real driving force for the horizontal flow of a phase is the gradient in the Gibbs free energy, which is a function of saturation, specific interfacial area, and fluid pressure. Thus, in addition to the pressure gradient, gradients in saturation and specific interfacial area also appear in the generalized Darcy's law. This means that it is, in principle, possible to maintain gradients in pressure and saturation under no-flow condition. Since few studies of the generalized formula exist, we only included the saturation gradient as a new driving force to reduce uncertainties in the estimation of parameters. The model for one-dimensional horizontal flow is defined by the following set of equations consisting of continuity equations for the water phase and the specific interfacial area as well as the generalized Darcy's law (Niessner and Hassanizadeh, 2008; Pop et al., 2009):

$$\phi\frac{\partial S_w}{\partial t}+\frac{\partial q_w}{\partial x}=0 \qquad [7]$$

$$\frac{\partial a_{wa}}{\partial t}+\frac{\partial\left(a_{wa}w_{wa}\right)}{\partial x}=E_{wa} \qquad [8]$$

$$q_w=-\frac{k_{rw}k}{\mu_w}\left(\frac{\partial p_w}{\partial x}-\lambda\frac{\partial S_w}{\partial x}\right) \qquad [9]$$

$$k_{rw} \quad S_e \qquad [10]$$

where q_w is the Darcy flow velocity, k denotes the intrinsic permeability, k_{rw} is relative permeability, μ_w is the viscosity of water, λ is a material property, w_{wa} is the macroscopic flux of the specific interfacial area, δ is the exponent for the relative permeability, and E_{wa} is the net production rate of the specific interfacial area.

Hassanizadeh and Gray (1993b) proposed the following Darcy type equation for the flux of fluid–fluid interfaces:

$$w_{wa}=-k_{wa1}\left[\frac{\partial\left(a_{wa}\sigma_{wa}\right)}{\partial x}+\psi_{wa}\frac{\partial S_w}{\partial x}\right] \qquad [11]$$

where k_{wa1} represents the interfacial permeability, ψ_{wa} is a material coefficient, and σ_{wa} denotes the average interfacial tension. Since σ_{wa} is constant for air–water interfaces at constant temperature, Eq. [11] simplifies to the following:

$$w_{wa}=-k_{wa1}\sigma_{wa}\left(\frac{\partial a_{wa}}{\partial x}+\frac{\psi_{wa}}{\sigma_{wa}}\frac{\partial S_w}{\partial x}\right)=-k_{wa}\left(\frac{\partial a_{wa}}{\partial x}+\Omega\frac{\partial S_w}{\partial x}\right) \qquad [12]$$

in which k_{wa} and Ω are adjusted material properties that include the effect of the average interfacial tension.

Compared with the model of Niessner and Hassanizadeh (2008) and Pop et al. (2009), we employed a simpler relationship for the production term. Based on the analysis given in Appendix A1, the following relationship was used for the production term E_{wa}:

$$E_{wa}=-\kappa\frac{\partial a_{wa}}{\partial p_c}\frac{\partial S_w}{\partial t} \qquad [13]$$

The above system of equations (i.e., Eq. [5–13]) can be solved numerically in terms of the two primary variables: S_w and p_c. The solution still requires certain continuity conditions at the contact surface between the two domains where saturation is discontinuous. For the water phase, we assumed continuity in the water flux and the pressure across the contact surface between the wet and dry domains. For the air–water interface, we assumed continuity in the interfacial area flux, $a_{wa}w_{wa}$. One more condition is still needed to obtain a complete description of the interfacial area model. This was done by specifying continuity in the Gibbs free energy for the air–water interfaces. The corresponding expression of continuity is derived in Appendix A2. Hence, the model imposed continuity in $lna_{wa}+\Omega S_w/a_{wa}$ across the contact surface. As boundary conditions, we assigned zero fluxes for both water and the interfacial areas.

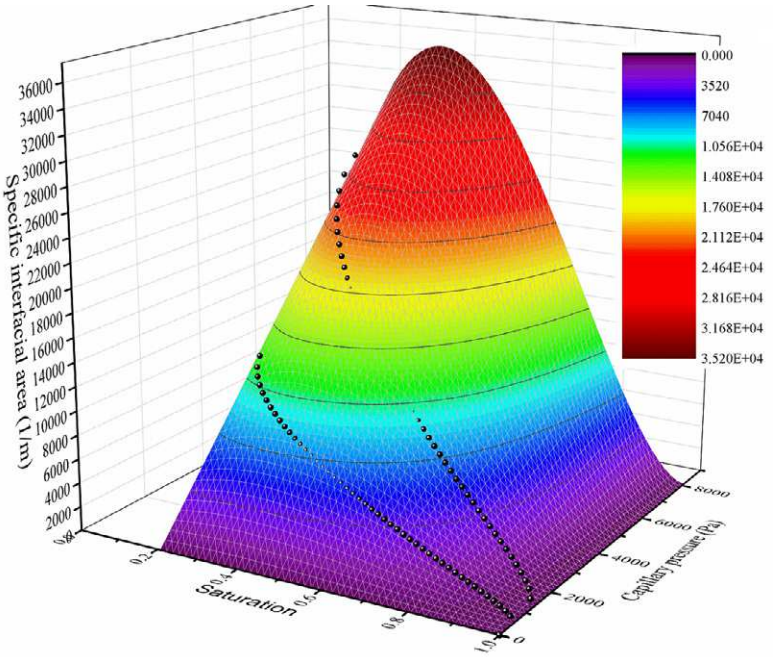

Fig. 4. Three-dimensional surface of capillary pressure, saturation, and specific interfacial area.

Table 2. Values of the coefficients in Eq. [5]

Parameter	Value	Standard error
a	24.60	3.685
b	1.73	0.275
c	1.00	0.017
R^2	0.992	

The full set of equations describing the interfacial area model was solved numerically by means of COMSOL Multiphysics 4.4 (COMSOL, 2014). A small grid size of 0.001 m was employed to achieve mesh-independent solutions. An adaptive time-step size was used based on a residual error of 10^{-6}. The equations were solved for both the dry and wet domains and coupled with each other by continuity conditions across the contact surface as explained earlier.

Numerical Results

We performed two sets of simulations using both the standard model and the interfacial area model. For one set, we assumed uniform initial conditions (albeit with different initial saturations for the dry and wet sides). The purpose of this set of simulations was to compare predictions obtained with the two modeling approaches. For the second set, we assigned nonuniform initial conditions corresponding to the measured data. Results of this set of simulations were compared with experimental data.

Simulations with the Richards Equation: Uniform Initial Conditions

Two different simulations were performed with the Richards equation: with and without hysteresis. We recognize that the simulations are relatively standard, but they are included in this paper to provide a comparison with the interfacial area model. Uniform initial saturation values of 0.23 and 0.70 were assigned to the dry and wet sides, respectively. The sand was assumed to be in an imbibition state initially, consistent with the manner in which the flume was packed. For the nonhysteretic case, we used the main imbibition p_c–S_w curve for both sides. For the hysteretic case, we used the main imbibition curve for the dry side and the main drainage curve for the wet side.

Figures 5a and 5b show calculated saturation and water pressure profiles as obtained with the Richards equation without accounting for capillary hysteresis. Results show that the initial saturation and water pressure discontinuities disappeared as soon as redistribution started. A significant change in saturation in both sides is evident already after 0.5 d. The entire system was essentially at equilibrium after only 1 d, with the final saturation distribution being uniform over the entire domain. Clearly, the numerical results in Fig. 5a and 5b, obtained with the Richards equation without hysteresis, are very much at odds with typical observations such as the measurements shown in Fig. 1 and 3.

Figure 5c and 5d show similar saturation and water pressure distributions when considering hysteresis. At the contact surface, saturations of the wet and dry sides decreased and increased, respectively, almost immediately to values that remained nearly constant in time. Equilibrium distributions in both sides were reached within ~1 d. This is contrary to the experimental data (Fig. 1), which show that complete equilibrium was probably not reached even after 30 d. Figure 5c clearly shows the persistence of the saturation discontinuity when hysteresis was included in the Richards equation. While different saturation distributions were obtained for the nonhysteretic and hysteretic cases, water pressure profiles and their changes in time were comparable. The time scale of change in the calculated saturation and pressure distributions, however, was much faster than the observations.

An interesting simulation result for the hysteretic case is that the saturation gradient was found to persist in the dry part even at equilibrium, which is in agreement with the observed data. The reason is that saturation of the soil in the dry side close to the contact surface increased dramatically at first but then started to decrease. We selected two points in the dry side to illustrate this difference in saturation. Figure 6a shows saturation values vs. time at two locations in the initially dry side (−10 and −35 cm). Saturation at −10 cm increased rapidly to 0.38 but thereafter decreased slowly to reach a final value of about 0.37. This point, hence, was first subject to imbibition and then to slow drainage until the redistribution process covered the entire dry side. By comparison, the point at −35 cm only exhibited imbibition. Hence, the two points followed different capillary pressure saturation scanning branches, leading to different saturations even though the final pressure values were the same as shown in Fig. 5d.

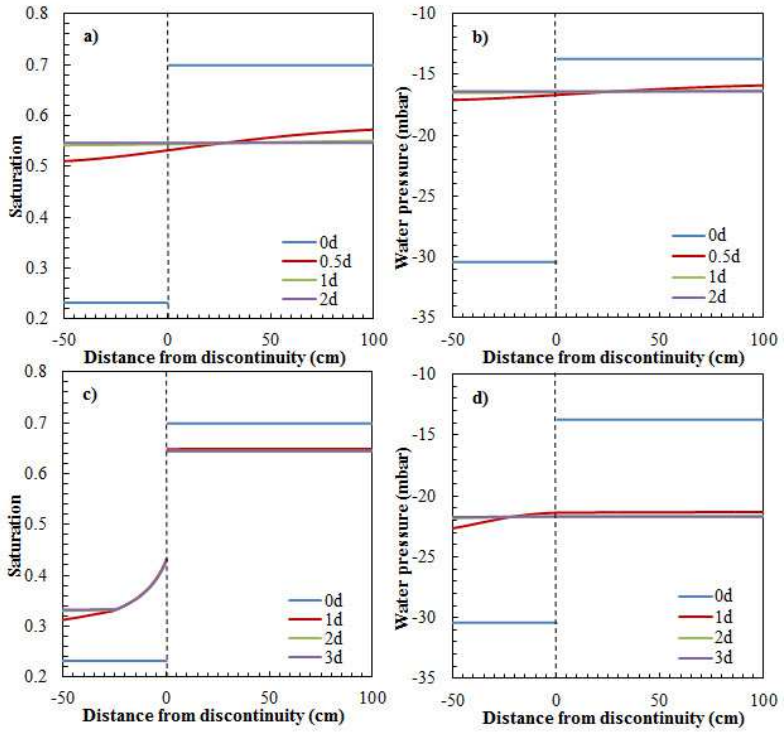

Fig. 5. Saturation and water pressure distributions along the entire domain simulated with the Richards equation (a, b) without and (c, d) with accounting for hysteresis.

Simulations with the Interfacial Area Model: Uniform Initial Saturation

We performed two sets of simulations with the interfacial area model to show the type of saturation and pressure distributions it prescribed. In one case, we assumed that applicability of the standard Darcy's law (i.e., with $\lambda = 0$ in Eq. [9]); in the other case we used the generalized Darcy's law ($\lambda \neq 0$).

As initial conditions, we specified the same uniform saturation values in each side as used for the HYDRUS calculations. For the interfacial area model, we also needed to specify initial pressure distributions. These were chosen to be also uniform in each side and obtained from the imbibition curve corresponding to the initial saturation values. A single p_c–S_w–a_{wa} surface was used for both the dry and wet sides. The set of equations defining the interfacial area model contains five parameters (k_{wa}, Ω, κ, δ, and λ). For our simulations, we chose parameter values used in several earlier studies (notably Niessner and Hassanizadeh, 2008). These were: $k_{wa} = 10^{-17}$ m^3 s^{-1}, $\Omega = 4000$ m^{-1}, $\kappa = 3 \times 10^4$ Pa, $\delta = 3$, and $\lambda = 2 \times 10^4$ Pa.

Figures 7a and 7b show the calculated distributions of saturation and the water pressure, respectively, using the standard Darcy's law ($\lambda = 0$). Redistribution of water in both sides occurred mostly within 2 d, with the entire domain reaching equilibrium within 3 d. The saturation discontinuity at the contact surface persisted despite the fact that a single p_c–S_w–a_{wa} surface was used for both sides.

Results of simulations with the generalized Darcy's law ($\lambda \neq 0$) are shown in Fig. 7c and 7d. Saturation in the dry side increased much more gradually, while a significant gradient remained in the water pressure distribution, even after 3 d. Hence, the generalized Darcy's formulation ($\lambda \neq 0$) produced a much lower water flux, which increased the required equilibration time as compared with the standard Darcy formulation ($\lambda = 0$). An important result here is that saturation is uniform along each side at equilibrium. Thus, contrary to the standard model, the interfacial area model does not produce a nonuniform saturation distribution in the dry side, which is not in agreement with experiments. We further illustrate in Fig. 6b the saturation changes vs. time at the same points (−10 and −35 cm) in the dry side as before for the Richards equation. Compared with the standard model (Fig. 6a), qualitatively similar (but lower) saturation distributions were obtained, except the identical saturation values were reached at the two points (−10 and −35 cm) at equilibrium.

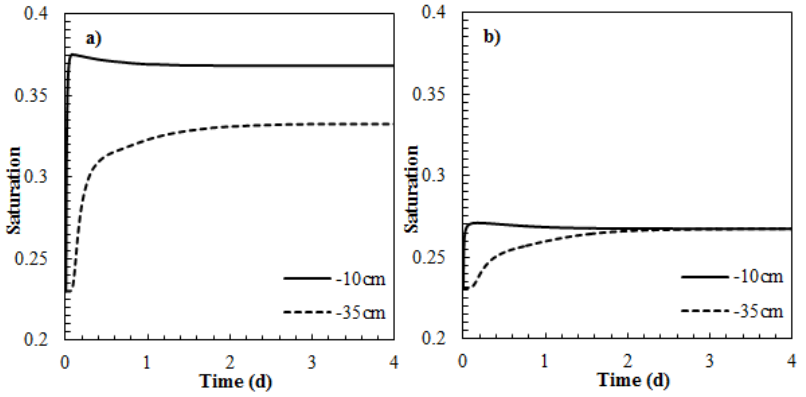

Fig. 6. Calculated saturation values versus time at −10 and −35 cm (the dry side) using (a) the standard model with hysteresis and (b) the interfacial area model using the standard Darcy's law.

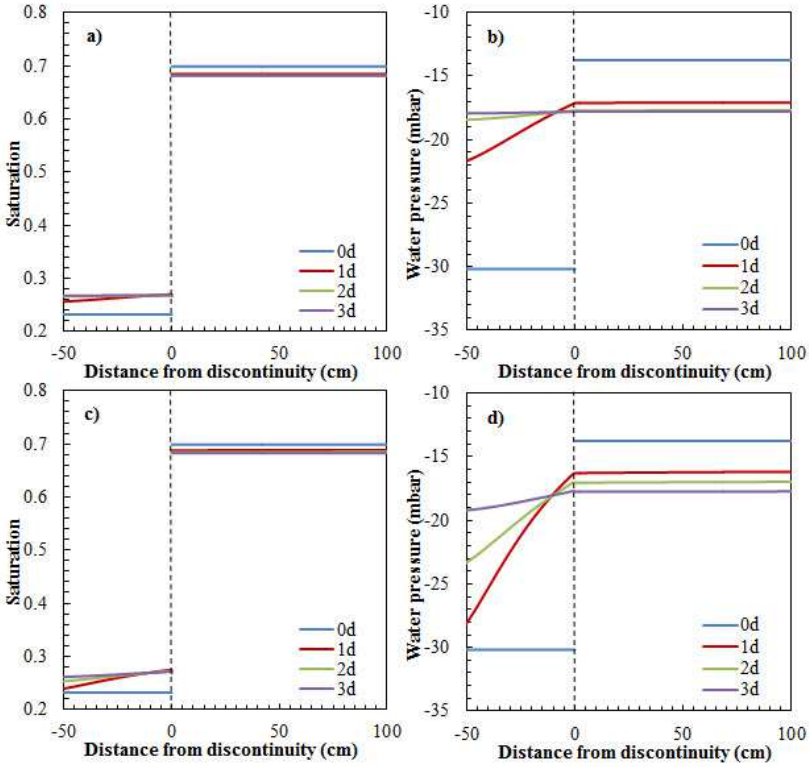

Fig. 7. Saturation and water pressure distributions along the entire domain simulated with the interfacial area model using (a, b) the standard Darcy's law and (c, d) the generalized Darcy's law.

Simulations with Both Models: Spatially Variable Initial Saturation Distributions

In these simulations, we first used the experimentally measured initial water saturation distributions to prescribe initial conditions. We again assumed that initially the sand was everywhere in an imbibition state, consistent with the way in which the flume was packed. Moreover, based on the nonuniform bulk density distribution measured along the flume (see Fig. 1), we assigned different values for porosity to each segment of 5 cm along the flume. This

approach would account for the heterogeneity in the sand packing. Regarding the initial condition in HYDRUS, we could specify either the water content or the pressure distributions. The latter could be calculated from measured initial saturation values using the main imbibition curve.

Results of the HYDRUS simulations are shown in Fig. 8. The colored solid lines and dots represent numerical results and experimental data, respectively. Different colors indicate different measurement times. When saturation was used as the initial condition for the heterogeneous flume, it produced unrealistic pressure gradients at the start of the simulations ($t = 0$). On the other hand, when we used a uniform pressure head as the initial condition, simulation results were found to be far from the observed saturation data given in Fig. 8b. These inconsistencies could not be resolved, as there was a lack of information about the initial state of various points along the flume.

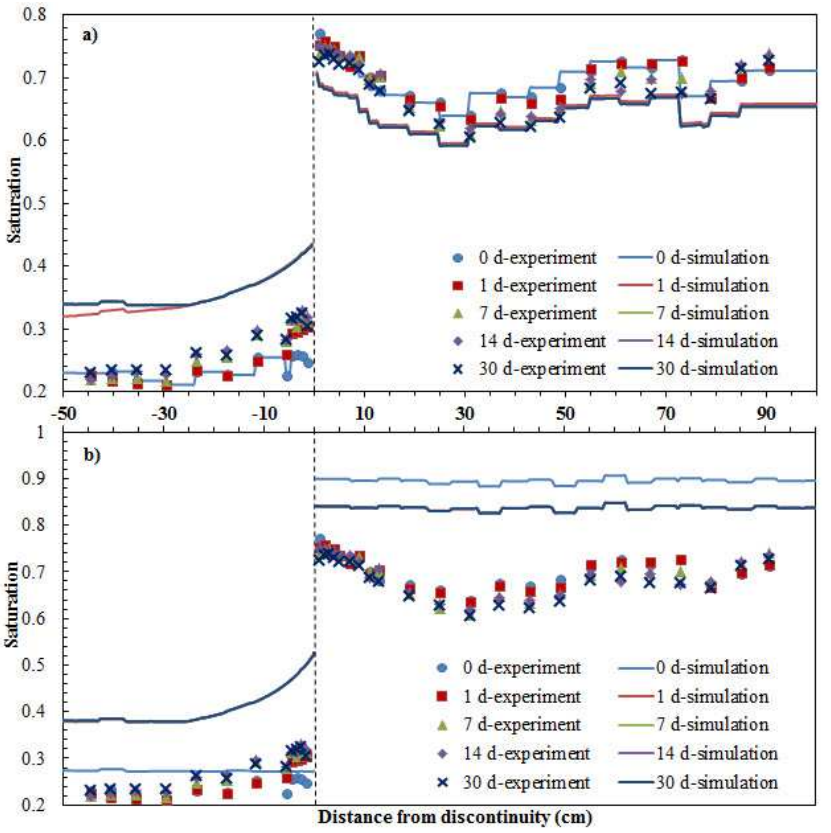

Fig. 8. Observed saturation profiles and fitted curves obtained with the standard Richards equation using (a) saturation or (b) pressure as the initial condition.

The simulation results in Fig. 8, obtained with the standard Richards equation, deviated substantially from the experimental data in the dry side. Saturations there increased much faster and remained much higher than the measured values. We tried to remedy this situation by modifying the relative permeability curve to generate lower flow rates. For this purpose, we increased the value of exponent l in Eq. [3], while keeping the other parameters as their measured values. Results are shown in Fig. 9a. It is evident that the redistribution process was now much slower, but that saturations near the contact surface in the dry side were still too high. The only way we could force the simulation results to match the experimental data was to significantly increase the value of the coefficient α of the imbibition curve. When the value of α was increased by a factor of 2, good agreement was obtained with the measured saturations as shown in Fig. 9b.

Next, the interfacial area model with the generalized Darcy's law was employed. For this model, we needed to specify not only the initially measured saturation distribution but also the initially measured water pressure distribution. Regarding the parameter values, we equated the porosity φ and the saturated conductivity K_s to their measured values (see Table 1). Also, one p_c–S_w–a_{wa} surface was assigned to both dry and wet sides. The parameter values (a, b, and c) for this surface are given in Table 2. Auxiliary simulations showed that the results were not sensitive to changes in the values of the interfacial area flux parameters k_{wa} and Ω. We hence fixed these values to 10^{-17} m^3 s^{-1} and 4000 m^{-1}, respectively, as used in our preliminary simulations. The three remaining parameters were determined by fitting to the data: λ in the generalized Darcy's equation, Eq. [9]; the exponent δ of the relative permeability function, Eq. [10]; and the coefficient κ of interfacial area production term in Eq. [13].

Calculated saturation profiles and measured data at different measurement times with the interfacial area model are shown in Fig. 9c. The model was found to perform best using fitted values of $\kappa = 5 \times 10^4$ Pa, $\delta = 4.69$, and $\lambda = 10^4$ Pa. Results compared well with the experimental data in the dry side, including the now much slower progression toward equilibrium and the spatial distribution of saturation observed (see Fig. 9c).

Discussion, Conclusions, and Outlook

In this study we have simulated a horizontal water redistribution experiment recently conducted by Feuring et al. (2014). Two different models, the standard Richards equation and an interfacial area model, were employed and compared in terms of their ability to reproduce the experimental data. The Richards equation was used with and without accounting for hysteresis, while for the interfacial area model, we used two different formulations for Darcy's law.

As expected, the standard model without hysteresis gives results that were at odds with the observations. In particular, the Richards

equation produced a full redistribution of water and the complete disappearance of the saturation discontinuity between the two sides of the experimental setup. The hysteretic Richards model did lead to nonuniform saturation distribution and properly simulated the saturation discontinuity. However, the flow process was found to be much faster than observed, while saturation values in the dry side were severely overpredicted. The differences could be minimized only if unrealistic values were assigned to some of the soil hydraulic parameters.

The interfacial area model produced better agreement with the observed spatial and temporal saturation distributions. To some extent this was expected since this model contains a larger number of parameters. Nevertheless, the fact that the interfacial area model predicted the persistence of the discontinuity in saturation, using the same set of hydraulic properties for both sides, is encouraging.

Compared with having eight possible parameters in the standard model (i.e., φ, K_s, α-imbibition, α-drainage, n-imbibition, n-drainage, S_{wr}, and l), the interfacial area model contains eleven parameters (i.e., φ, K_s, a, b, c, δ, S_{wr}, λ, Ω, k_{wa}, and κ). Hence, the interfacial area model has more flexibility in fitting the observed data. We must point out that in the case of the standard model, only α-imbibition and l were determined by fitted the experimental data, and in the case of the interfacial area model, only three parameters, namely δ, λ, and κ, were determined. The other parameters were either measured or determined indirectly. Both models were able to describe the experimental data vs. time and spatially after optimization. The unrealistic adjustment of some of the values of the soil hydraulic properties were needed for the Richards equation, however, is a concern. At the same time, while the interfacial area model provided an excellent description of the data, it is still unclear how realistic the adopted values of κ and λ were. Additional experiments are very much needed to determine the appropriateness of these values.

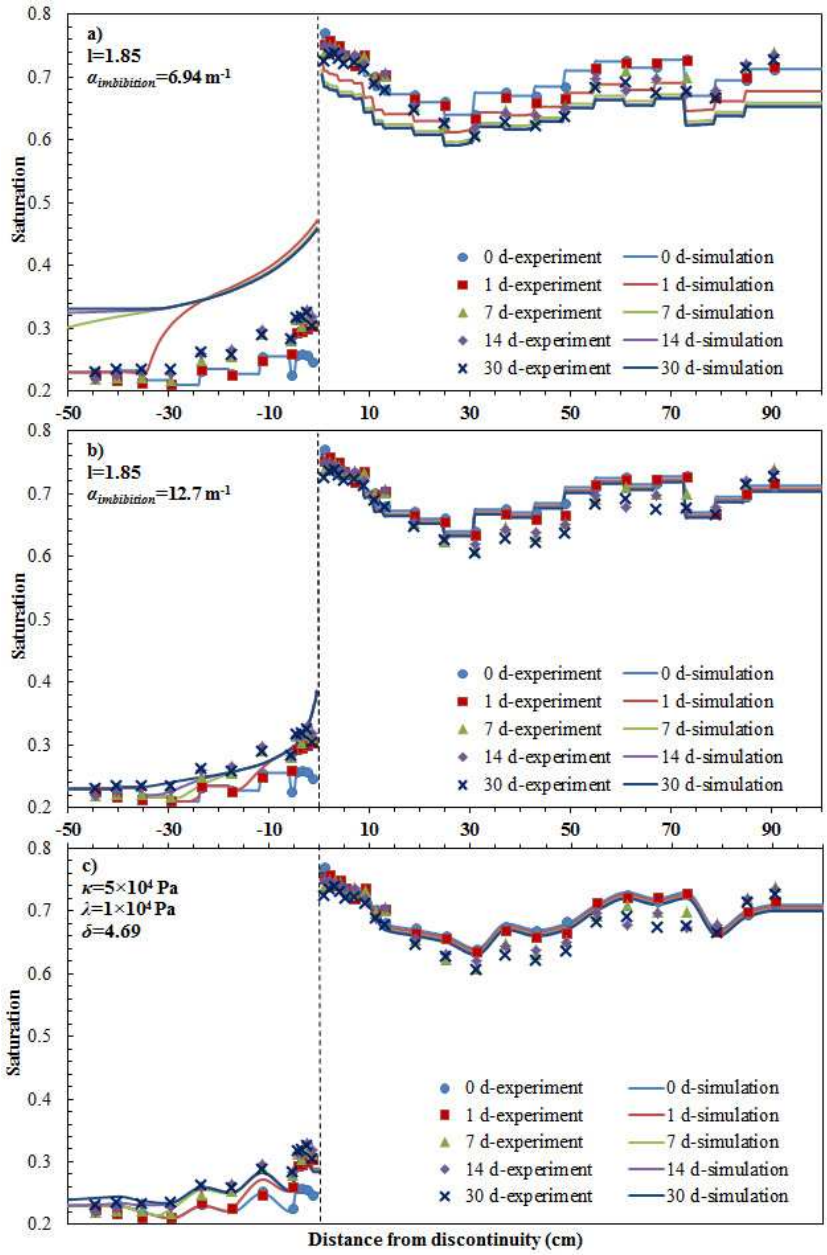

Fig. 9. Observed saturation profiles and fitted curves using the standard Richards equation with (a) adjusted values of l, (b) l and α-imbibition, and (c) the interfacial area model.

The detailed comparisons of the classical Richards model, the interfacial area model, and the experimental data provided much insight into the fundamentals of the two models. The introduction of the specific interfacial area eliminated the need for knowing the historical path of water flow and its dynamics. Meanwhile, it is clear that the interfacial area model still contains several assumptions and uncertainties, requiring further evaluation before this model can be more widely applied in practical application of multiphase flow.

Finally, we acknowledge that additional horizontal (and vertical) redistribution experiments and analysis of the interfacial area model are needed in the future. First, like in our study, better-controlled experiments must be performed to ensure homogeneous soil packing and direct measurement of initial conditions. This will reduce uncertainties in the experimental data and theoretical analysis. Second, independent experimental measurements should be conducted to obtain the p_c–S_w–a_{wa} surfaces, the interfacial permeability, and the interfacial area production term. Also, several material properties appearing in the interfacial mass balance equation and the generalized Darcy's law should be determined. Finally, long-term experiments should be conducted until full equilibrium is reached.

Appendix A1: Production Rate Term of the Specific Interfacial Area

A constitutive equation is needed for the rate of production (or destruction) of the specific interfacial area E_{wa}, in Eq. [8]. We know that the interfaces will be created or destroyed if capillary equilibrium is not reached. As explained in Hassanizadeh and Gray (1993a), capillary equilibrium will be disturbed if the difference in average fluid pressures deviates from the average capillary pressure. This is implicit in the dynamic capillarity equation (Hassanizadeh and Gray, 1993a; Hassanizadeh et al., 2002):

$$p_a - p_w = p_c - \tau \frac{\partial S_w}{\partial t} \quad [A14]$$

where τ, often called the dynamic capillarity coefficient, is a material property that may depend on saturation. One way to parameterize E_{wa} is to relate this parameter to the degree of the deviation from capillarity equilibrium. Thus, we proposed that E_{wa} is proportional to the difference in the amount of interfacial area, a_{wa}, under dynamic and static conditions. Since a_{wa} is a function of S_w and p_c (see Eq. [5]), we postulate the following linear relationship for E_{wa}:

$$E_{wa} = \kappa_1 \left[a_{wa}(S_w, p_a - p_w) - a_{wa}(S_w, p_c) \right] \quad [A15]$$

where κ_1 is a material coefficient. We next expand the function $a_{wa}(S_w, p_a - p_w)$ in a Taylor series around p_c to obtain the following:

$$a_{wa}(S_w, p_a - p_w) \approx a_{wa}(S_w, p_c) + \frac{\partial a_{wa}(S_w, p_c)}{\partial p_c}(p_a - p_w - p_c) \quad [A16]$$

Substitution of Eq. [A14] into [A16] and combination of the results with [A15] will lead to the following:

$$E_{wa} = -\kappa_1 \tau \frac{\partial a_{wa}}{\partial p_c}\frac{\partial S_w}{\partial t} = -\kappa \frac{\partial a_{wa}}{\partial p_c}\frac{\partial S_w}{\partial t} \quad [A17]$$

where $\partial a_{wa}/\partial p_c$ can be obtained from Eq. [5] and κ has to be determined experimentally. In this study, we estimated the value of κ by fitting this parameter to the observed data.

Appendix A2: Gibbs Free Energy for the Specific Interfacial Area

As explained in the main text, at the contact surface between dry and wet domains, we require continuity in the Gibbs free energy of air–water interfaces. The Gibbs free energy for air–water interfaces, G_{wa}, is defined as (e.g., Hassanizadeh and Gray, 1993b; Eq. 50b):

$$G_{wa} = A_{wa} - \frac{\sigma_{wa}}{\Gamma_{wa}} \quad [A18]$$

where Γ_{wa} and A_{wa} are the average mass density and macroscopic Helmholtz free energy of air–water interfaces, respectively. The Helmholtz free energy is known to be a function of S_w, a_{wa}, and Γ_{wa} (if the latter is not constant). In particular, the macroscopic interfacial tension, Γ_{wa}, is related to the change in the Helmholtz free energy as a result in a change in the specific interfacial area (see e.g., Hassanizadeh and Gray, 1993b; Eq. 26):

$$\sigma_{wa} = -a_{wa}\Gamma_{wa}\left(\frac{\partial A_{wa}}{\partial a_{wa}}\right) \quad [A19]$$

The differential of G_{wa} is found next from Eq. [A18]:

$$dG_{wa} = \frac{\partial A_{wa}}{\partial a_{wa}} da_{wa} + \frac{\partial A_{wa}}{\partial S_w} dS_w - \frac{1}{\Gamma_{wa}} d\sigma_{wa} \quad [A20]$$

where we have considered the average mass density of interfaces to be constant. Substituting Eq. [A19] into [A20] and collection of terms results in the following:

$$dG_{wa} = -\frac{d(a_{wa}\sigma_{wa})}{a_{wa}\Gamma_{wa}} + \frac{\partial A_{wa}}{\partial S_w} dS_w \quad [A21]$$

From Hassanizadeh and Gray (1993b) and the definition of coefficient Ω in Eq. [12], we find:

$$\Omega = -\frac{\Gamma_{wa} a_{wa}}{\sigma_{wa}}\frac{\partial A_{wa}}{\partial S_w} \quad [A22]$$

Substitution of Eq. [A22] into [A21] gives the following:

$$dG_{wa} = -\frac{d(a_{wa}\sigma_{wa})}{a_{wa}\Gamma_{wa}} - \frac{\Omega \sigma_{wa}}{a_{wa}\Gamma_{wa}} dS_w \quad [A23]$$

An approximate integration of this relationship yields the following:

$$G_{wa} = -\frac{\sigma_{wa}}{\Gamma_{wa}}\left(\ln a_{wa} + \Omega \frac{S_w}{a_{wa}}\right) + G_0 \quad [A24]$$

where G_0 is a constant of integration. Here again, we have assumed that Γ_{wa} is a constant. Thus, the continuity in the Gibbs free energy of air–water interfaces across the contact surface requires continuity in $\ln a_{wa} + \Omega S_w / a_{wa}$.

Acknowledgments

The first author is funded by the China Scholarship Council. The authors would like to thank the Associate Editor Robert Schwartz and Insa Neuweiler for a comprehensive review of the manuscript and for comments that helped to improve it.

References

Always, F.J., and V.L. Clark. 1911. A study of the movement of water in a uniform soil under artificial conditions. Annual Report 25:246–287 Nebraska Exp. Station, Lincoln, NE.

Biswas, T.D., D.R. Nielsen, and J.W. Biggar. 1966. Redistribution of soil water after infiltration. Water Resour. Res. 2:513–524. doi:10.1029/WR002i003p00513

Chen, L., and T.C.G. Kibbey. 2006. Measurement of air–water interfacial area for multiple hysteretic drainage curves in an unsaturated fine sand. Langmuir 22:6874–6880. doi:10.1021/la053521e

Chen, D., L.J. Pyrak-Nolte, J. Griffin, and N.J. Giordano. 2007. Measurement of interfacial area per volume for drainage and imbibition. Water Resour. Res. 43:W12504.

COMSOL. 2014. COMSOL Multiphysics 4.4. COMSOL Inc., Burlington, MA.

Dane, J.H., and P.J. Wierenga. 1975. Effect of hysteresis on the prediction of infiltration, redistribution and drainage of water in layered soil. J. Hydrol. 25:229–242. doi:10.1016/0022-1694(75)90023-2

Everett, D.H. 1954. A general approach to hysteresis, part 3: A formal treatment of the independent domain model of hysteresis. Trans. Faraday Soc. 50:1077–1096. doi:10.1039/tf9545001077

Feuring, T. 2010. Horizontal redistribution of two fluid phases in a porous medium. M.S. thesis. Stuttgart University, Germany.

Feuring, T., J. Braun, B. Linders, G. Bisch, S.M. Hassanizadeh, and J. Niessner. 2014. Horizontal redistribution of two fluid phases in a porous medium: Experimental investigations. Transp. Porous Media 105:503–515. doi:10.1007/s11242-014-0381-9

Haines, W.B. 1930. Studies in the physical properties of soil. V. The hysteresis effect in capillary properties and the modes of moisture distribution associated herewith. J. Agric. Sci. 20:97–116. doi:10.1017/S002185960008864X

Hassanizadeh, S.M., M.A. Celia, and H.K. Dahle. 2002. Dynamic effect in the capillary pressure-saturation relationship and its impacts on unsaturated flow. Vadose Zone J. 1:38–57. doi:10.2136/vzj2002.3800

Hassanizadeh, S.M., and W.G. Gray. 1990. Mechanics and thermodynamics of multiphase flow in porous media including interphase boundaries. Adv. Water Resour. 13:169–186. doi:10.1016/0309-1708(90)90040-B

Hassanizadeh, S.M., and W.G. Gray. 1993a. Thermodynamic basis of capillary pressure in porous media. Water Resour. Res. 29:3389–3405. doi:10.1029/93WR01495

Hassanizadeh, S.M., and W.G. Gray. 1993b. Toward an improved description of the physics of two-phase flow. Adv. Water Resour. 16:53–67. doi:10.1016/0309-1708(93)90029-F

Held, R.J., and M.A. Celia. 2001. Modelling support of functional relationships between capillary pressure, saturation, interfacial area and common lines. Adv. Water Resour. 24:325–343. doi:10.1016/S0309-1708(00)00060-9

Jaynes, D.B. 1984. Comparison of soil-water hysteresis models. J. Hydrol. 75:287–299. doi:10.1016/0022-1694(84)90054-4

Joekar-Niasar, V., and S.M. Hassanizadeh. 2011. Specific interfacial area: The missing state variable in two-phase flow equations? Water Resour. Res. 47:W05513.

Joekar-Niasar, V., and S.M. Hassanizadeh. 2012. Uniqueness of specific interfacial area-capillary pressure-saturation relationship under non-equilibrium conditions in two-phase porous media flow. Transp. Porous Media 94:465–486. doi:10.1007/s11242-012-9958-3

Joekar-Niasar, V., S.M. Hassanizadeh, and A. Leijnse. 2008. Insights into the relationships among capillary pressure, saturation, interfacial area and relative permeability using pore-network modeling. Transp. Porous Media 74:201–219. doi:10.1007/s11242-007-9191-7

Karadimitriou, N.K., S.M. Hassanizadeh, V. Joekar-Niasar, and P.J. Kleingeld. 2014. Micro-model study of two-phase flow under transient conditions: Quantifying effects of specific interfacial area. Water Resour. Res. 50:8125–8140. doi:10.1002/2014WR015388

Kona, S. 1997. Experimental investigation of horizontal redistribution of water in unsaturated porous media. M.S. thesis. University of Minnesota, Minneapolis.

Kool, J.B., and J.C. Parker. 1987. Development and evaluation if closed-form expression for hysteretic soil hydraulic properties. Water Resour. Res. 23:105–114. doi:10.1029/WR023i001p00105

Lenhard, R.J., and J.C. Parker. 1991. Comparing simulated and experimental hysteretic two-phase transient fluid flow phenomena. Water Resour. Res. 27:2113–2124. doi:10.1029/91WR01272

Luckner, L., M.Th. van Genuchten, and D.R. Nielsen. 1989. A consistent set of parametric models for the two-phase flow of immiscible fluids in the subsurface. Water Resour. Res. 25:2187–2193. doi:10.1029/WR025i010p02187

Marshall, F. 2009. Numeric solution of Philip's redistribution problem. M.S. thesis. Stuttgart University, Germany.

Mualem, Y. 1974. A conceptual model of hysteresis. Water Resour. Res. 10:514–520. doi:10.1029/WR010i003p00514

Mualem, Y. 1984. A modified dependent domain theory of hysteresis. J. Soil Sci. 137:283–291. doi:10.1097/00010694-198405000-00001

Niemet, M.R., M.L. Rockhold, N. Weisbrod, and J.S. Selker. 2002. Relationships between gas-liquid interfacial surface area, liquid saturation, and light transmission in variably saturated porous media. Water Resour. Res. 38:10-1–10-12.

Niessner, J., and S.M. Hassanizadeh. 2008. A model for two-phase flow in porous media including fluid-fluid interfacial area. Water Resour. Res. 44:W08439.

Parker, J.C., and R.J. Lenhard. 1987. A model for hysteretic constitutive relations governing multiphase flow: 1. Saturation pressure relations. Water Resour. Res. 23:2187–2196. doi:10.1029/WR023i012p02187

Peck, A.J. 1971. Redistribution of soil water after infiltration. Soil Res. 9:59–71. doi:10.1071/SR9710059

Pham, H.Q., D.G. Fredlund, and S.L. Barbour. 2005. A study of hysteresis models for soil-water characteristic curves. Can. Geotech. J. 42:1548–1568. doi:10.1139/t05-071

Philip, J.R. 1964. Similarity hypothesis for capillary hysteresis in porous materials. J. Geophys. Res. 69:1553–1562. doi:10.1029/JZ069i008p01553

Poulovassilis, A. 1962. Hysteresis of pore water—An application of the concept of independent domains. J. Soil Sci. 93:405–412. doi:10.1097/00010694-196206000-00007

Poulovassilis, A., and W.M. El-Ghamry. 1978. The dependent domain theory applied to scanning curves of any order in hysteretic soil water relationships. J. Soil Sci. 126:1–8. doi:10.1097/00010694-197807000-00001

Pop, I.S., C.J. van Duijn, J. Niessner, and S.M. Hassanizadeh. 2009. Horizontal redistribution of fluids in a porous medium: The role of interfacial area in modeling hysteresis. Adv. Water Resour. 32:383–390. doi:10.1016/j.advwatres.2008.12.006

Šimůnek, J., M. Šejna, H. Saito, M. Sakai, and M.T. van Genuchten. 2009. The HYDRUS-1D software package for simulating the one-dimensional movement of water, heat and multiple solutes in variably-saturated media. Dep. Envir. Sci., Univ. of California, Riverside.

Scott, P.S., G.J. Farquhar, and N. Kouwen. 1983. Hysteretic effects on net infiltration. Advances in Infiltration 11–83:163–170.

Staple, W.J. 1969. Comparison of computed and measured moisture redistribution following infiltration. Soil Sci. Soc. Am. J. 33:840–847. doi:10.2136/sssaj1969.03615995003300060015x

Talsma, T. 1974. The effect of initial moisture content and infiltration quantity on redistribution of soil water. Soil Res. 12:15–26. doi:10.1071/SR9740015

Topp, G.C. 1971. Soil-water hysteresis: The domain theory extended to pore interaction conditions. Soil Sci. Soc. Am. Proc. 35:219–225. doi:10.2136/sssaj1971.03615995003500020017x

Vachaud, G. 1969. Étude d'une redistribution après l'arrêt d'une infiltration horizontale. In: P.E. Rijtema and H. Wassink, editors, Water in the unsaturated soils, Proc. Int. Symp. Wageningen, 19–25 June 1969. Int. Assoc. of Sci. Hydrology and UNESCO, Belgium.

Vachaud, G., and J. Thony. 1971. Hysteresis during infiltration and redistribution in a soil column at different initial water contents. Water Resour. Res. 7:111–127. doi:10.1029/WR007i001p00111

van Genuchten, M.Th. 1980. A closed-form equation for predicting the hydraulic conductivity of unsaturated soils. Soil Sci. Soc. Am. J. 44:892–898. doi:10.2136/sssaj1980.03615995004400050002x

Werner, A.D., and D.A. Lockington. 2006. Artificial pumping errors in the Kool–Parker scaling model of soil moisture hysteresis. J. Hydrol. 325:118–133. doi:10.1016/j.jhydrol.2005.10.012

Youngs, E.G. 1958. Redistribution of moisture in porous materials after infiltration: 2. Soil Sci. 86:202–207. doi:10.1097/00010694-195810000-00006

Youngs, E.G., and A. Poulovassilis. 1976. The different forms of moisture profile development during the redistribution of soil water after infiltration. Water Resour. Res. 12:1007–1012. doi:10.1029/WR012i005p01007